Nitrogen Hydrate Cage Occupancy and Bulk Modulus Inferred from Density Functional Theory-Derived Cell Parameters

C. Métais, C. Petuya, S. Espert, J. Ollivier, L. Martin-Gondre, A. Desmedt

Nitrogen Hydrate Cage Occupancy and Bulk Modulus Inferred from DFT-derived Cell Parameters

C. Métais[a,b,c], C. Petuya[b], S. Espert[b,d], J. Ollivier[c], L. Martin-Gondre[a,*], A. Desmedt[b,*]

a) Institut UTINAM, UMR 6213 CNRS, Université de Bourgogne - Franche-Comté, Besançon, France
b) Groupe Spectroscopie Moléculaire, Institut des Sciences Moléculaires (ISM), UMR 5255 CNRS, Université de Bordeaux, France
c) Groupe Spectroscopie, Institut Laue Langevin (ILL), Grenoble, France
d) Donostia International Physics Center (DIPC), Paseo Manuel de Lardizabal 4, 20018 San Sebastián, Spain

* Corresponding authors : arnaud.desmedt@u-bordeaux.fr ; ludovic.martin@univ-fcomte.fr

Abstract. Gas clathrate hydrates solid materials, ubiquitous in the nature as found either on the ocean floor, permafrost on earth or in extraterrestrial planets and comets, are also technologically relevant, e.g., for energy storage or carbon dioxide sequestration. Nitrogen hydrate, in particular, is of great interest as a promoter of the kinetics of methane replacement reaction by carbon dioxide in natural gas hydrates. This hydrate may also appear in the chemistry of planets wherever the nitrogen constitutes the majority of the atmosphere. A fine understanding of the stability of this hydrate under various thermodynamic conditions is thus of utmost importance to assess its role in the many fields where it occurs. In the present work we have investigated the structural properties of the nitrogen hydrate by means of DFT calculations. We show that the lattice parameters strongly depend onto the cage occupancy and that sI structure has higher bulk elasticity than sII structure. An energy analysis reveals the key role played by the cage occupancy onto the type of hydrate structure formed, that could be used for experimentally estimating the cage occupancy through the lattice parameter measurement.

I. Introduction

Gas clathrate hydrates are natural porous solid materials. Since few decades, they became of particular interest for their applications in various research fields, such as energy, technology and environment.[1-3] As examples, gas hydrates are involved in flow assurance, in gas separation technologies or for desalination and they are considered as a substantial energy reservoir.[1-3] These systems are also studied from a fundamental point of view in the areas of physical-chemistry and astrophysics.[2-3] Nitrogen hydrate has been widely studied due to its particular relevance. For example, a new technology has been developed for the replacement of methane by carbon dioxide in natural gas hydrates, using N_2 as a promoter of the replacement kinetics.[4] The investigation of nitrogen hydrates is also relevant in the fields of atmospheric chemistry and in astrophysics, since nitrogen is one of the most abundant constituents of the atmosphere of various planets in our solar system. Researches conducted in that fields rely on clathrate hydrates to explain and reconstruct the evolution of the atmospheric composition, either on Earth[5-10] and on planets or comets, such as 67P/Churyumov-Gerasimenko[11].

Clathrate hydrates are composed of water molecules, arranged in cages forming the host network. Small gas molecules trapped in these cages are referred to as guest molecules. Nitrogen hydrate is known to crystallize into the so-called type I and type II cubic structures (called sI and sII), lattices with unit cell parameter of approximately 12 Å and 17 Å, respectively. The sI and sII unit cells consist of 46 and 136 water molecules, respectively. Both structures are composed of two types of cages, commonly called small cages and large cages (labeled SC and LC, respectively). The sI contains 2 pentagonal dodecahedra (noted 5^{12}) SCs and 6 tetradecahedron ($5^{12}6^2$) LCs while the sII is made of 16 SCs (5^{12}) and 8 hexakaidecahedral ($5^{12}6^4$) LCs. The small cages are the same in both structures, but the large cages in sII are slightly bigger than in sI. Thermodynamic modeling of nitrogen hydrate predicted that sI would be the most stable form at high pressures (>1000 bar) while sII would be more stable at lower pressures (~100 bar)[12], as shown in Fig. 1. Experimentally, it has been proved that, at moderate pressure, nitrogen hydrate initially forms a type I structure and transforms into its thermodynamically stable form, the type II structure, after few days.[13] Similar structural metastability has been observed for carbon monoxide clathrate hydrate, which also forms in sI and converts into sII after 17 weeks.[14,15] Small molecules, like N_2 or CO, preferentially form the type II structure due to their ability to fill the larger SCs proportion in sII when compared to sI. It becomes then of great interest to investigate how the cages occupancy by the guest molecules influence the gas hydrate structural stability.

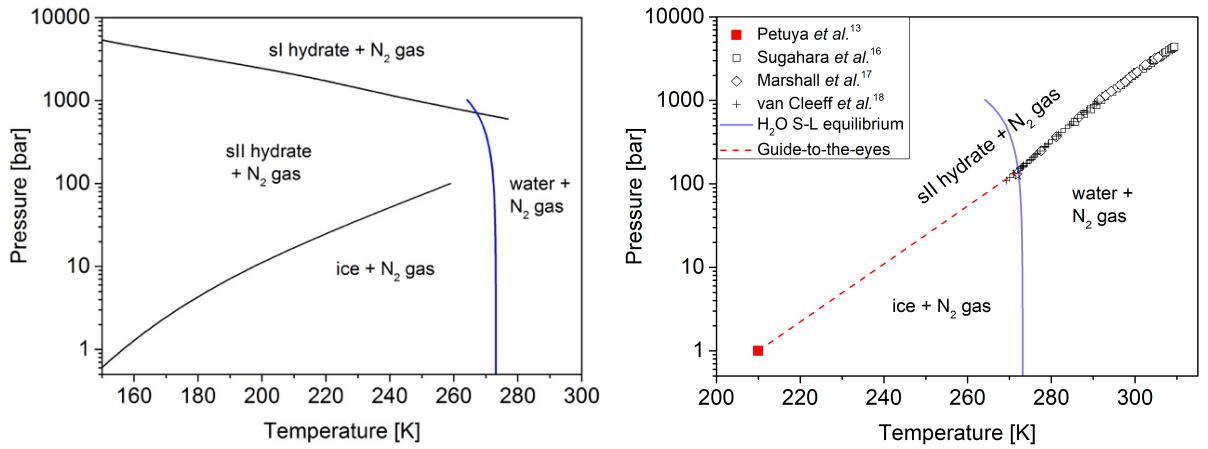

Figure 1. Theoretical (left) and experimental (right) nitrogen hydrate phase diagrams. Black solid lines correspond to calculated nitrogen hydrate equilibrium lines adapted from Lundgaard, et al [12]. The blue line corresponds to the melting equilibrium of water. Black symbols correspond to experimental data.[16-18] The red square is the dissociation point of the nitrogen hydrate measured experimentally at 1 bar.[13]

The cage occupancy corresponds to the average number of guest molecules in small or large cages. For instance, empty sI SCs correspond to $\theta_{SC} = 0$ (all SC empty) and one guest molecule per sI SC correspond to $\theta_{SC} = 1$ (all SCs filled). Experimental studies with various techniques have been conducted to investigate the occupancy θ_{SC} and θ_{LC} of small and large cages, respectively, in nitrogen clathrate hydrates.[4,8,10,13,19,20] These studies revealed that N_2 molecules were localized in both types of cages, regardless of the structure formed. Notably, neutron diffraction studies showed that a sII nitrogen hydrate formed at 150 bar and 258 K for 20 days had $\theta_{SC} = 0.87$ and $\theta_{LC} = 1.2$ (meaning that 20% of the sII LCs are occupied by two nitrogen molecules)[19] and that a sI nitrogen hydrate formed at 1093 bar and 268 K for 11 days had $\theta_{SC} = 0.98$ and $\theta_{LC} = 1.12$ [4]. Overall, SC occupancy ranges from 82 to 100 % and LC occupancy ranges from 97 to 125 %. The LC double occupancy has almost always been observed for samples studied by neutron diffraction. A Raman scattering study of the nitrogen hydrate recently evidenced that the LCs have the ability to catch and release guest molecules by simply varying T-P conditions.[13] This ability was also observed in the case of the carbon monoxide hydrate.[15] The effect of both the temperature and pressure on cage occupancy and lattice parameter of nitrogen hydrates has been described. In general, for a given temperature, the cage occupancy increases with increasing pressure[13,21] and, at fixed pressure, the cage occupancy increases when the temperature increases[13,22]. However, at a given pressure, the lattice parameter increases with temperature[13,19], whereas decreases with the pressure (for P>500bar) at constant temperature[8,10]. Studying these effects of pressure on lattice parameters has also led to the determination of the compressibility of the nitrogen hydrate. Experimentally, the structure type I has a lower bulk modulus B_T than structure type II,[8,10] meaning that sI may undergo more structural deformations than sII.

Several theoretical studies of the nitrogen hydrate have also been conducted. Molecular dynamics calculations were performed on sII nitrogen hydrate to investigate the possibility of LCs double occupancy.[23,24] These calculations showed that the hydrate structure remained stable for all tested pressures, temperatures and compositions. The volume and energies were found to be linearly dependent on the cage occupancy, and there was no marked difference in the structure between singly and doubly occupied systems. Grand-canonical Monte-Carlo studies were performed on sI and sII nitrogen clathrate hydrates.[25,26] These studies showed that at low temperature (at 50K), the SCs are filled before the LCs, but at higher temperature (at 150K) the opposite happens, i.e. the LCs are filled before the SCs. Carbon monoxide hydrate has also been simulated and, in the latter case, whatever the structure formed or the temperature, the SCs were always occupied before the LCs, although at 150 K the occupancy of both types of cages becomes simultaneous.

All these results highlight the key role of cage occupancy, and in particular the importance of water-guest interactions on the structural stability of the hydrate.[27] However, as important as they are, these water-guest interactions cannot be considered alone to fully describe the structural and energetic properties of the system.[28] Indeed, it is important to consider the host-host interactions contained in the H-bonded solid network formed by the water molecules that are the main constituent of a gas hydrate.[29] As an example, the encapsulation of strong acids within the water cages leads to generate H-bond defects (breaking the so-called ice rule) within the water network modifying the H-bonded water dynamics [30-32] and physico-chemical properties such as hydrate stability[33] or formation kinetics[34]. The structural stability of the nitrogen hydrate must therefore be investigated considering both guest-host and host-host interactions.

Nowadays, to study molecular interactions in condensed phase systems, it is appropriated to use periodic density functional theory (DFT) calculations.[35] Two types of interactions are involved in gas hydrates: the host-host interactions between water molecules, which correspond to hydrogen bonding, and the guest-host interactions between the guest molecule and the host cage, which is mainly due to van der Waals (vdW) dispersion forces. It is important that DFT correctly describes these two kinds of interactions and in particular the vdW interactions that contribute to the structural stabilization of the hydrate with respect to ice. Unfortunately, the most common exchange-correlation functionals in DFT, such as local density approximation (LDA) or generalized gradient approximation (GGA), are not able to describe the long-range electron correlations that are responsible for the dispersion forces. Although many dispersion-based DFT methods have been developed over the recent years[36], there is not yet a method fully capable to provide an accurate description of clathrate hydrates[28,37].

DFT-based clathrate hydrates structural stability studies have been reported recently.[38,39] In the first study[38], DFT has been used in order to determine the equilibrium lattice volume and bulk modulus of sII hydrocarbons hydrates using several functionals and equations of state with a comparison to experimental

data. This investigation concluded that the experimental lattice parameters are better reproduced by using the revPBE functional (revised Perdew-Burke-Ernzerhof), and the bulk modulus of sII hydrate was found to increase with increasing atomic volume. In the second study[39], DFT calculations have been performed to investigate the structural stability and energy properties of the carbon monoxide hydrate. The simulations were done on complete sI and sII unit cells, with varying cage occupancy, and testing two functionals (PBE[40] and vdW-DF[41]) to study the impact of the dispersion forces on the gas hydrates properties. Optimized lattice parameters were compared to neutron diffraction and a good agreement was found between theoretical and experimental results. The hydrate structural stability was also investigated through a careful potential energy analysis and results showed that sII is the thermodynamically stable CO hydrate structure. Furthermore, increasing the CO content in the hydrate, i.e. doubly occupying the LCs, was found to destabilize the sI and to have a stabilizing effect on the sII.

The aim of the present study is to investigate the structural and energetic properties of nitrogen clathrate hydrate. Both sI and sII unit cells are considered, and DFT-derived structural properties are compared to experimental data. An analysis of the DFT potential energies is presented and aims at providing a better understanding of the hydrate structural stability. Two different exchange-correlation functionals are used, namely the semilocal functional Perdew-Burke-Ernzerhof (denoted PBE) and the nonlocal functional vdW-DF. The PBE functional does not include dispersion effects but still provide a correct description of the H-bonding network. Therefore, the comparison with the vdW-DF functional, which accounts for dispersion interactions, allows to investigate the effect of the dispersion forces on the calculations. Since the hydrate structural stability depends on the presence of the guest molecules (empty hydrate is not stable), the influence of the cage occupancy on structural and energetic properties is also evaluated.

II. Calculations Details

The *Vienna ab initio Simulation Package* (VASP 5.3.5), a periodic plane wave basis set code[42-45], has been used to perform DFT calculations. In order to calculate the exchange-correlation energy, two functionals were used: the semilocal PBE functional[40] and the nonlocal van der Waals Density Functional (vdW-DF)[41]. Using both functionals made it possible to investigate how the dispersion forces influence the calculated properties. The projector augmented waves (PAW) method[46,47] has been used to describe the electron core interaction. The energy cutoff in the plane wave expansion was 520 eV corresponding to high precision VASP calculations. All calculations are made at the Γ point of the Brillouin zone because of the large size of unit cells.

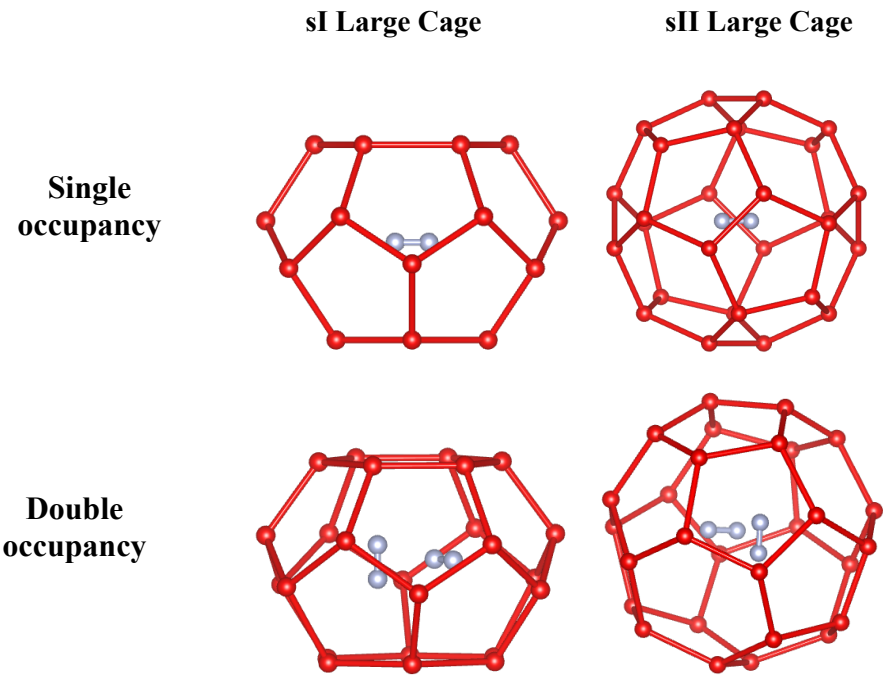

Figure 2. Representation of sI (Left) and SII(Right) LC for single N_2 occupancy (Top) and double (Bottom) N_2 occupancy.

The first step of the DFT calculations consisted in building the elementary simulation box. The simulation box was built using X-ray diffraction data[48,49] of the sI and sII structures, providing the oxygen atoms positions of the aqueous sub-structure. Two hydrogens atoms were then added to each oxygen atom to form the water molecules and build the water cages by following the ice rules (i.e. each water molecules accepts and donates 2 H-bonds). Simulations were performed on a complete cubic unit cell with a size of approximately 12.0 Å and 17.2 Å for sI and sII, respectively. The influence of the cage occupancy on the structural and energetic properties of nitrogen hydrate has been investigated. The performed simulations are labelled according to cage occupancy as $[\theta_{SC}/\theta_{LC}]$, where θ_{SC} and θ_{LC} are the small cage and large cage occupancies respectively. A summary of all the studied cases is presented in Table 1. The first calculations were performed on singly occupied systems, i.e. with all cages occupied by one guest only, which was positioned at the center of the cages (Fig. 2). These calculations are labelled [1/1] according to the above convention. Calculations have also been performed on systems with some doubly occupied large cages (i.e. $\theta_{LC} > 1$), keeping a single occupation of the small cages (i.e. $\theta_{SC} = 1$). The double occupancy of the large cages has been varied from one large cage doubly occupied (i.e. $1 < \theta_{LC} < 2$) to all the large cages doubly occupied (i.e. $\theta_{LC} = 2$). In the case of a doubly occupied large cage, the guest nitrogen molecules were positioned as follows: the molecular axis were positioned orthogonally at a distance of 2.4Å (corresponding to 1/3 of the LC diameter) from each other (Fig. 2) with the center of mass of the two molecules corresponding to the center of the cage. As an example, Fig. 2 illustrates singly and doubly occupied large

cages of sI and sII. Finally, various incompletely filled systems with empty cages were tested (i.e. $\theta_{SC} \leq 1$ or $\theta_{LC} \leq 1$].

Once the simulation box was built, a first relaxation of all atomic positions was performed to minimize the energy of the structure. Then a volume relaxation step was carried out in order to determine the optimum lattice parameter of each simulated system. A final global relaxation of the complete unit cell was done until forces on atoms converged to within 0.01 eV/Å. For each case studied, both sI and sII have been considered with the two functionals (PBE and vdW-DF). In order to verify our initial H-bonded water arrangement, a set of calculations has been performed with the initial structure arrangement provided by Takeuchi et al.[50] The test was realized on simply occupied nitrogen hydrates (sI and sII) with both functionals used to run the calculations. All energy values obtained were very close to the ones calculated with the present built simulation box.

Table 1. Summary of the calculations performed. In each case, both PBE and vdW-DF functionals have been used.

sI clathrate structure			sII clathrate structure		
Labelling	Occupancy		Labelling	Occupancy	
[$\boldsymbol{\theta}_{SC}$/$\boldsymbol{\theta}_{LC}$]	$\boldsymbol{\theta}_{SC}$	$\boldsymbol{\theta}_{LC}$	[$\boldsymbol{\theta}_{SC}$/$\boldsymbol{\theta}_{LC}$]	$\boldsymbol{\theta}_{SC}$	$\boldsymbol{\theta}_{LC}$
[0/1]	0	1	[0/1]	0	1
[0.5/1]	0.5	1	[0.5/1]	0.5	1
[1/0]	1	0	[1/0]	1	0
[1/0.5]	1	0.5	[1/0.5]	1	0.5
[1/1]	1	1	[1/1]	1	1
[1/1.17]	1	1.17	[1/1.125]	1	1.125
[1/1.33]	1	1.33	[1/1.25]	1	1.25
[1/1.5]	1	1.5	[1/1.375]	1	1.375
[1/1.67]	1	1.67	[1/1.5]	1	1.5
[1/1.83]	1	1.83	[1/1.625]	1	1.625
[1/2]	1	2	[1/1.75]	1	1.75
			[1/1.875]	1	1.875
			[1/2]	1	2

III. Results and Discussion

1) DFT-derived structural properties

Unit cell volume optimizations were performed for all the simulated systems. These optimizations were done by varying lattice parameters using a 0.2 Å step and relaxing all atomic positions. In Fig. 3 examples of calculated vdW-DF potential energy curves are presented as a function of the lattice parameter for both type I and type II structures and for different cage occupancies (PBE functional results are provided in Fig. S1). These potential energies were successfully fitted using the Birch-Murnaghan equation of state (denoted EOS)[51]

$$E(V) - E_0 = \frac{9V_0B_T}{16}\left\{\left[\left(\frac{V_0}{V}\right)^{2/3} - 1\right]^3 B_T' + \left[\left(\frac{V_0}{V}\right)^{2/3} - 1\right]^2 \left[6 - 4\left(\frac{V_0}{V}\right)^{2/3}\right]\right\} \quad (1)$$

where E_0 corresponds to the minimum energy associated with the volume V_0, B_T is the bulk modulus and B_T' is the derivative of the bulk modulus with respect to pressure. The optimal lattice parameter of the cubic structure deduced from these fits was then used to perform the final relaxations and extract properties discussed in the following.

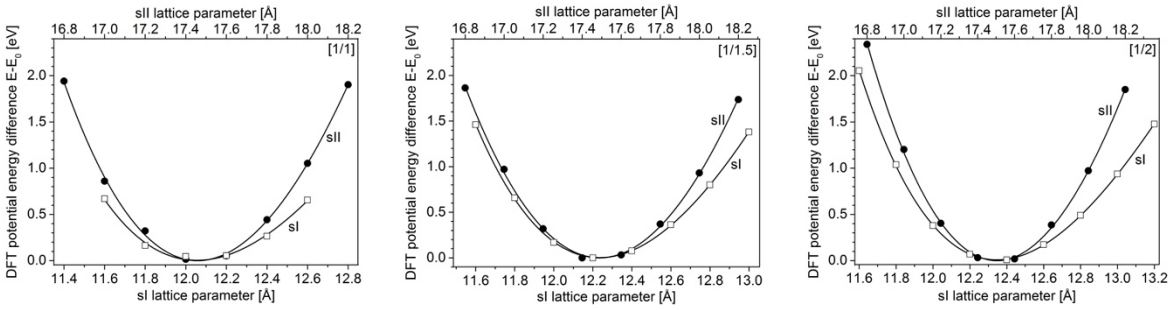

Figure 3. DFT potential energy difference E-E$_0$, as a function of the lattice parameter from DFT calculations obtained with the vdW-DF functional for both sI (empty squares) and sII (filled circles) structures. The results are shown for all cages single-occupancied (left, [1/1]), for half of the LCs double-occupied (center, [1/1.5]) and for all LCs double-occupied (right, [1/2]). The continuous lines represent the fitted curves using the Birch-Murnaghan equation of state (see Equation (1)).

The dependence of the unit cell parameter on the large cage and small cages occupancies is shown in Fig. 4 for sI and sII structures. The optimal lattice parameters obtained with the vdW-DF functional (empty symbols) are larger than the one obtained with the PBE functional (solid symbols), for both structures. Such a behavior has been reported in the case of methane[28] and carbon monoxide[39] hydrates: the vdW-DF functional lead to overestimate the interatomic distances (and thus overestimate the lattice parameter)

compared to PBE functional due to the repulsive nature of the exchange-correlation contribution of the vdW-DF functional[39]. The PBE-derived unit cell parameter increases with the cage occupancy, regardless of the considered structure and interestingly, a discontinuity in the lattice parameters slope is observed for $\theta_{LC} > 1$ (i.e. for double occupancy of the large cages). With the vdW-DF functional, the same trend is observed for the sI structure while the sII does not exhibit significant variations with the cage occupancy.

The lattice parameters presented in Fig. 4, resulting from DFT calculations, correspond to values obtained at zero temperature (no kinetics energy contribution is considered in the calculations) and minimized pressure as relaxed lattice parameters were considered (i.e. P ~ 0 bar). For a more appropriated comparison of the DFT-derived cell parameter with the experimental ones recorded at higher pressures (see Fig. 5), the parameters of the Birch-Murnaghan EOS are used to include the pressure effects in the calculation of the DFT-derived cell parameters. The Birch-Murnaghan EOS (see equation 1) - used to fit the potential energy dependence with volume of Fig. 3 - gives access to the bulk modulus B_T , i.e. the inverse of the relative volume variation of the material submitted to a pressure, expressed as:

$$B_T = -V\left(\frac{\partial P}{\partial V}\right)_{P=0} \quad (2)$$

The DFT-derived bulk moduli B_T of the N_2 hydrates (reported in Table 2) exhibit a general trend: PBE-calculated B_T are greater than the ones derived from vdW-DF, except for multiple LC occupancy of the sI structure. The variation range of bulk modulus values is also larger for the PBE functional. The overestimated distances for the vdW-DF functional lead to larger dimension of the cages compared with the PBE functional. Therefore, a smaller impact on the cage occupancy is observed for the vdW-DF functional thus giving a smoother evolution of the bulk moduli.

In order to compare with the DFT-derived bulk moduli, the experimental values are reported in the Table 3. The DFT-derived values are of the same order of magnitude as those measured experimentally with a better agreement for the most recent study.[10] Moreover, the sI bulk moduli are lower than those of sII for experimental results and for most cases in theoretical results. The lower B_T value measured in the case of structure sI reflects the fact that this structure has a higher elasticity (easier deformation with pressure) than the structure sII. In other words, the sII requires more energy to be deformed. This behavior agrees with the present DFT-derived results shown in Fig. 3: curvatures of the potential energies variation with the lattice constant are less pronounced for sI than for sII - a flatter curvature meaning a lower bulk modulus B_T. In addition, the volume variation, illustrated through the cage occupancy dependence of the cell parameter (Fig. 4), is more important for sI than for sII, with a pronounced deviation in the case of the PBE functional. This supports the observation that the structure sI is more impacted than the structure sII by the cage occupancy variation. In some limited cases, the calculated B_T values are lower for sII than for sI. This

happens mostly when the small cages are not fully occupied such as in the [0/1] and [0.5/1] cases. Since there are more empty SCs in sII than in sI, the sII structure becomes more deformable than the sI structure.

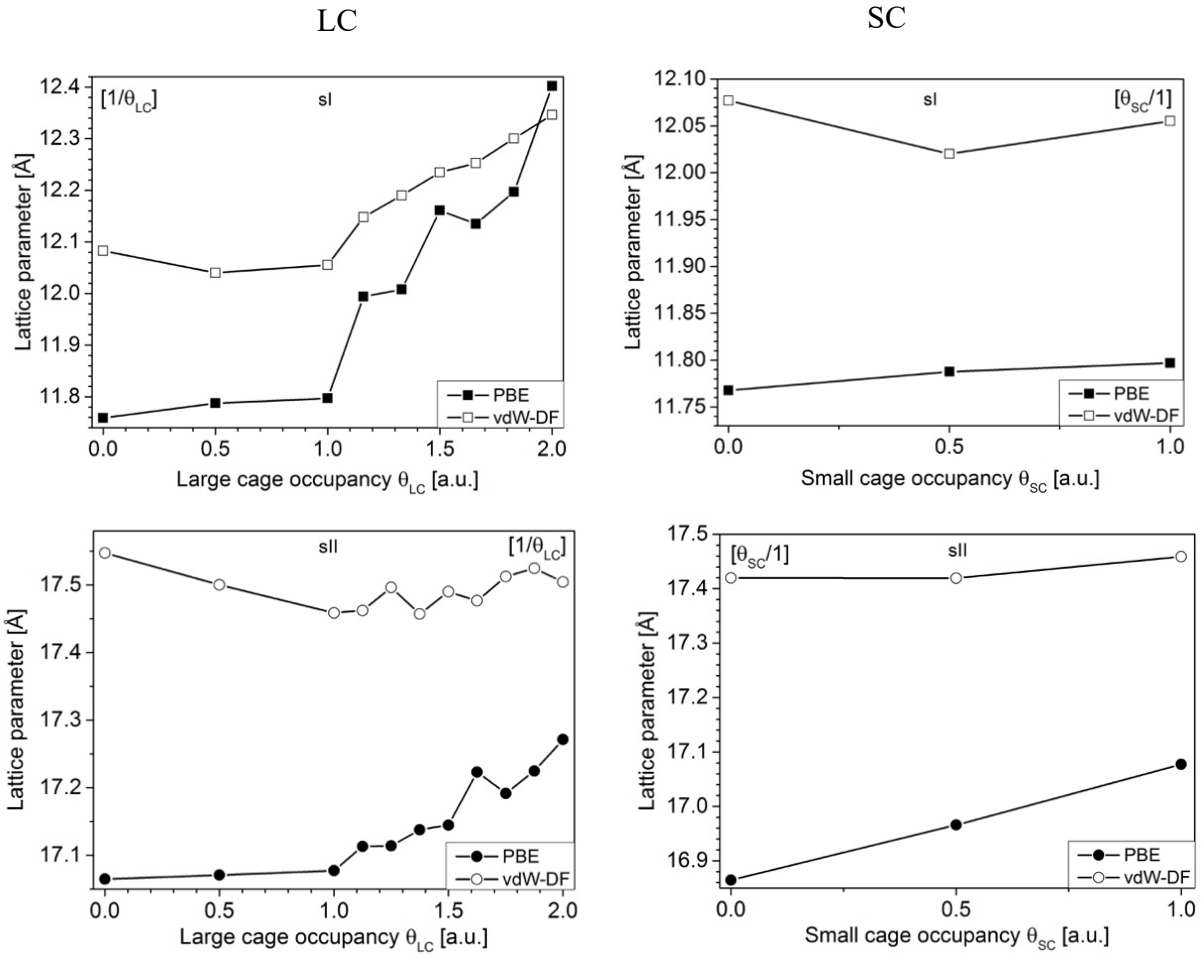

Figure 4. DFT-derived lattice parameter as a function of the large (left) and small (right) cage occupancy, for sI (at the top) and sII (at the bottom) structures. The solid and empty symbols correspond to the values obtained with the PBE and vdW-DF functionals, respectively.

There are only few experimental studies reporting an isothermal variation of the cage occupancy and unit cell parameter with pressure.[8,10,13] From Rietveld refinement[8,10] the small cage occupancy θ_{SC} has been reported to vary from 85 to 100% while the large cage occupancy θ_{LC} is almost always greater than or equal to 100%. The isothermal compressibility coefficient κ_T (inverse of the bulk modulus) has been used to calculate the DFT-derived cell parameters at pressures matching the experimental values and at cage occupancies (indicated with stars in Table 2) close to the experimentally reported values, for which it was assumed a SC occupancy of 1 in all cases. The Fig. 5 shows the DFT calculated cell parameters versus the large cage occupancy for a full SC occupancy (θ_{SC} = 1) of the sI and sII structures. The experimental cell

parameters determined from neutron diffraction are also reported on the same figure. As expected, the pressure-corrected theoretical data leads to lower lattice parameter for both functionals than the initially calculated at P = 0 bar. For pressures above 200 bar, the lattice parameter decreases with increasing pressure for both theoretical and experimental data, as expected from the compressibility of the material. It should be mentioned that the experimental values reported at 1 bar has been acquired at 80 K[13] while the other experimental data at higher pressures[8,10] were measured at 273 K. The pressure-corrected sI lattice parameter obtained with the vdW-DF functional is systematically larger than the experimental values while the PBE functional pressure-corrected lattice parameter is in excellent agreement. The same agreement has been reported in the case of carbon monoxide[39] and methane[28] hydrates, comforting the idea that the hydrogen-bonding network is correctly described with the PBE functional. In the case of the sII structure, both functionals lead to identical relative deviation (lower than 2.5%) from the experimental data.

Table 2. Theoretical bulk moduli extracted from DFT simulations data fitted with the Birch-Murnaghan equation of state. Values are given for sI and sII hydrates with both PBE and vdW-DF functionals. Standard deviation errors associated to the fitting procedure are indicated in parentheses. The values marked with stars are the ones used to correct the data shown in Fig. 5.

	PBE				vdW-DF			
Labeling	sI		sII		sI		sII	
[$\boldsymbol{\theta}_{SC}/\boldsymbol{\theta}_{LC}$]	B_T (kbar)		B_T (kbar)		B_T (kbar)		B_T (kbar)	
[0/1]	106.0	(0.6)	107.9	(1.3)	76.6	(0.7)	64.2	(3.3)
[1/0]	102.9	(4.0)	102.6	(0.5)	60.9	(9.6)	74.6	(0.8)
[0.5/1]	140.6	(10.1)	109.8	(1.6)	80.5	(1.4)	70.4	(1.1)
[1/0.5]*	100.0	(1.1)	100.6*	(0.1)	67.6	(3.3)	74.7*	(1.9)
[1/1]*	106.5*	(0.4)	100.3*	(0.2)	78.4*	(4.9)	80.4*	(1.4)
[1/1.125]*	-	-	99.3*	(0.3)	-	-	80.8*	(1.5)
[1/1.17]*	79.6*	(0.7)	-	-	74.7*	(1.9)	-	-
[1/1.25]*	-	-	98.5*	(0.3)			76.9*	(0.7)
[1/1.33]	84.0	(1.6)	-	-	75.5	(2.0)	-	-
[1/1.375]	-	-	100.4	(0.6)	-	-	74.0	(1.6)
[1/1.5]	64.8	(1.7)	98.1	(1.6)	86.1	(0.6)	75.5	(1.2)
[1/1.625]	-	-	86.2	(4.4)	-	-	70.7	(1.5)
[1/1.67]	82.1	(1.8)	-	-	83.0	(0.9)	-	-
[1/1.75]	-	-	101.2	(0.5)			86.5	(0.7)
[1/1.83]	68.1	(2.8)	-	-	82.6	(1.4)	-	-
[1/1.875]	-	-	93.0	(3.3)	-	-	84.9	(0.9)
[1/2]	58.9	(1.4)	98.1	(1.6)	79.3	(0.4)	86.6	(1.1)

Table 3. Experimental values of the bulk modulus B_T measured for N_2 hydrates of type I and type II structures[8,10].

Reference	Hydrate	T (K)	P (bar)	B_T (kbar)
8	N_2 D_2O SI	273	500 - 2500	25 - 42
	N_2 D_2O SII	273	500 - 2500	~115
10	N_2 D_2O SI	273	750 - 1000	79
	N_2 D_2O SII	273	150 - 1000	93

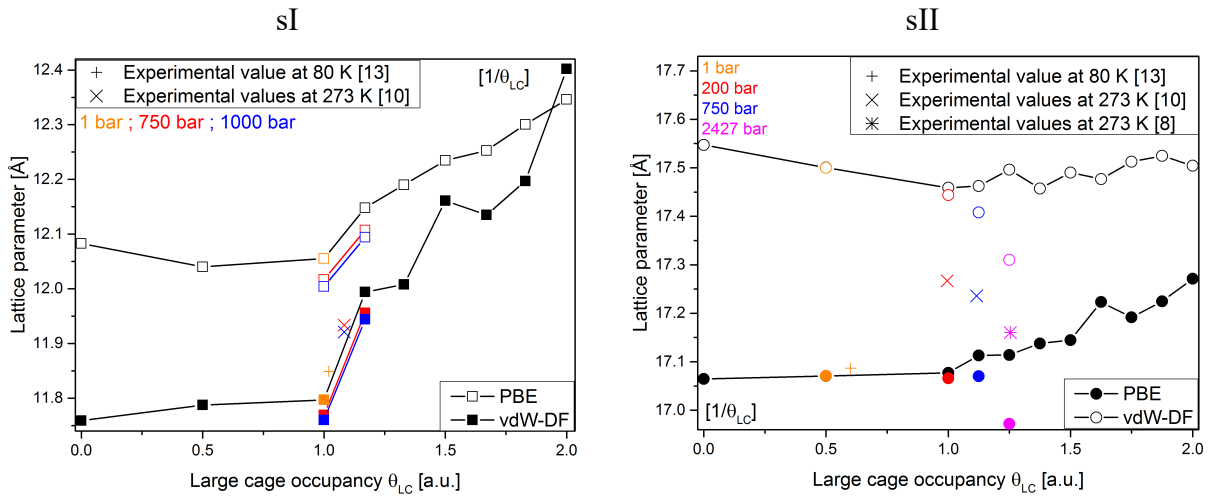

Figure 5. DFT-derived (black symbols) and compressibility-corrected (colored symbols) lattice parameter as a function of the large cage occupancy for sI (Left) and sII (Right). The solid and empty symbols correspond to the values obtained with the PBE and vdW-DF functionals, respectively. The crosses and asterisks correspond to experimental values measured at 273 K at several pressures (colored-indicated on the figure)[8,10] and the plus signs, to experimental values[13] measured at 80 K and 1 bar.

2) Potential energy analysis and hydrate stability.

As reported from time-dependent neutron diffraction analysis,[13] the nitrogen hydrate forms in the sI clathrate metastable structure and transforms into the thermodynamically stable sII clathrate structure for which the cage occupancy plays a role[20]. Such structural metastability involves different potential energies for the sI and sII structures. The nitrogen hydrate stability has been analyzed in terms of DFT-calculated

potential energies by following the methodology detailed in the work of Petuya *et al.*[39] The potential energy considered for the present analysis corresponds to intermolecular energies whose reference states are defined on the basis of the *intramolecular* energies of the isolated molecular species (water and nitrogen). The intermolecular cohesive energy provides information regarding the clathrate formation energy and corresponds to the non-bonding energy E^{NB}. It is decomposed into three main components: the host-host (HH) interactions E^{HH}, the guest-host (GH) interactions E^{GH} and the guest-guest (GG) interactions E^{GG}. E^{HH} is associated with the cohesive energy of the empty clathrate structure and corresponds to the H-bonding interactions between water molecules constituting the host substructure. The E^{GH} contribution, also known as binding energy, mainly corresponds to interactions between the guest molecules trapped inside the cages and the water molecules forming the cages. The guest-guest interaction E^{GG} - whose the contribution should be negligible at least for single occupation - is included into the calculated E^{GH}. These intermolecular energies have been computed for all sI and sII structures and cage occupancies reported in Table 1 using both PBE and vdW-DF functionals. To assess the influence of the cage occupancy variation on the calculated stabilization energies, representative results are presented as a function of the large cage occupancy in Fig. 6 for the vdW-DF functional that takes into account the dispersion forces. All calculated energies are reported in Table S1 and S2 for vdW-DF and PBE functionals, respectively.

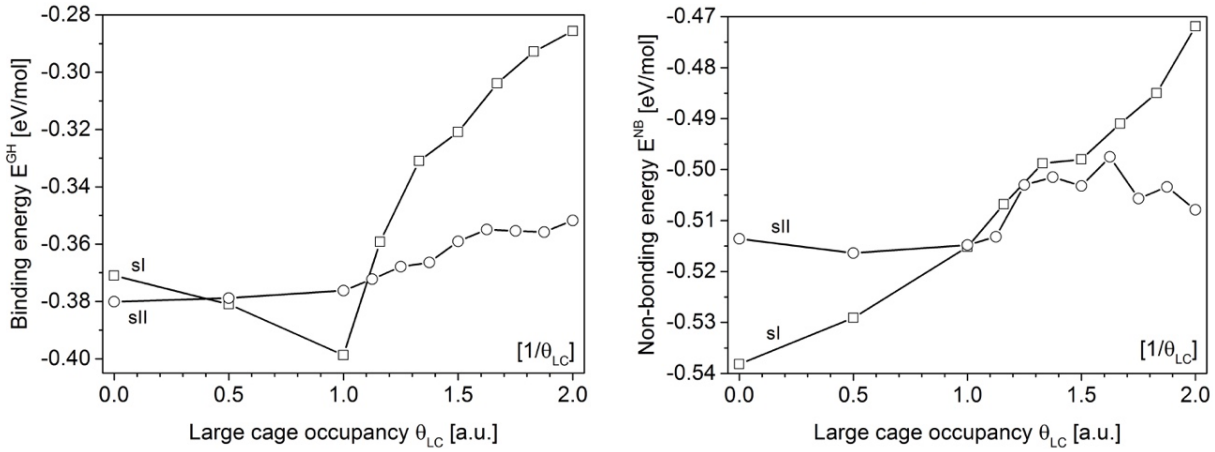

Figure 6. Guest-host energy E^{GH} (left) and nonbonding energy E^{NB} (right) as a function of the large cage occupancy θ_{LC} for sI (squares) and sII (circles) nitrogen hydrates, calculated with the vdW-DF functional. In all cases, the small cages are all simply filled.

The evolution of the binding energy E^{GH} is presented in Fig. 6 (left) as a function of the large cage occupancy θ_{LC}. Two regimes are visible on both sides at LCs occupancy $\theta_{LC} \sim 1$. Below this value, it is difficult to conclude about the preferred structure (sI or sII) in terms of binding energy. When the LCs are unoccupied (θ_{LC} =0 or [1/0]), the binding energy is weaker for sII than for sI. In other words, occupying only the SCs

stabilizes the sII. When the large cage occupancy increases close to one molecule per cage ($\theta_{LC} \sim 1$ or [1/1]), the binding energy becomes lower for sI than for sII. Above $\theta_{LC} \sim 1$, the large cages start to be doubly occupied and the binding energy increases for both structures with a more pronounced evolution for the sI structure than for the sII structure. Since the reported E^{GH} contains not only the water-nitrogen molecular interactions but also the guest-guest interactions, a destabilizing effect might be associated with the repulsive interactions becoming less negligible between two guests encapsulated within the same LC. The LC diameter being larger in sII than in sI,[1] the sII LCs better accommodate two guest molecules so that the sII structure becomes more favorable than the sI structure in terms of binding energy for $\theta_{LC} > 1$.

As previously described, it is necessary to consider the water-water interactions (E^{HH}) in addition to nitrogen-water interactions (E^{GH}) to fully analyze the hydrate structural stability: the water sub-structure is the major constituent in a hydrate and thus represent the major contribution to the stabilization energy. The nonbonding energy E^{NB} presented in Fig. 6 (right) shows again a difference on both sides of $\theta_{LC} \sim 1$. Below this value, E^{NB} is smaller for the sI structure than for the sII structure. For θ_{LC} ranging from *ca.*1 to *ca.* 1.5, sI and sII exhibit similar stability in terms of non-bonding energy and for $\theta_{LC} > 1.5$, the sII structure is clearly stabilized compared to the sI structure. The sI structure becomes less stable while increasing the LCs double occupancy: the non-bonding energy increases whereas the opposite happens for the sII structure.

IV. Conclusion

The nitrogen hydrate structural stability has been investigated by means of DFT calculations, performed using two different functionals: the semi-local PBE functional and the non-local vdW-DF functional in order to investigate the role of the dispersion forces on the structural stability of the clathrate. As experimentally shown,[8,10,13] the nitrogen hydrate can be form in the sI and sII structures depending on the thermodynamics conditions. In the present investigation, both structures were considered by simulating complete sI and sII unit cells with periodic boundary conditions. Experimentally, the cage occupancy has been proved to vary with the pressure and temperature.[8,10,13] The present DFT approach has thus included the influence of the cage occupancy onto the nitrogen hydrate structural stability and shown its key role played onto the formed hydrate structure. For both sI and sII structures, the DFT pressure-corrected lattice parameters are in good agreement (relative deviation lower than 2.5%) with experimental data.[8,10,13] The significant dependence of the calculated lattice parameters with the large cage occupancy thus shows that the lattice parameter measurement could constitute an experimental probe of the cage occupancy in nitrogen hydrate. The sI structure exhibits a more pronounced cage occupancy dependence of the lattice parameter than the sII structure. By analyzing the potential energy dependence of the DFT-derived lattice parameters with the

Birch-Murnaghan equation of state, the bulk modulii of both structures have been calculated for various cage occupancies and found to be in excellent agreement with those measured experimentally.[10] Moreover, the structural stability of the N_2 hydrate has been studied through a detailed analysis of the non-bonding potential energy. This analysis reveals that the large cage occupancy plays a key role in the type of formed clathrate structure (sI or sII). The nitrogen hydrate is preferentially formed in the sI structure for partial large cage occupancy, while the sI structure becomes less stable compared to the sII structure while increasing the double occupancy of large cages. For large cage occupancy greater than *ca.* 1.5, the sII structure becomes more stable than the sI structure. Such a result outlines the difference of elastic properties between the sI and sII structures: the bulk modulus is larger for sII than for sI, according to the measurements and the present DFT calculations.

Such theoretical energy analysis is in agreement with the structural metastability of gas hydrates recently evidenced, as well as with previous DFT calculations. Nitrogen hydrate initially forms in the sI structure that transforms into the sII structure after few days.[13,20] Carbon monoxide hydrate exhibits similar structural metastability as nitrogen hydrate, although its transformation from sI to sII is much longer and takes several weeks.[14,15] Experimentally, it has been shown that the LCs in both hydrates have the ability to catch and release guest molecules as the pressure and the temperature vary.[13,15,20] Together with previous DFT calculations performed on carbon monoxide hydrate,[14,39] the present investigation clearly underlines that the cage occupancy is the factor driving the stability, i.e. leading to the lower potential energy of the formed hydrate structure.

From partial occupancy to single occupancy of the LCs, the sI structure is the most stable structure, probably because the sI LCs are smaller than the sII LCs.[1] As soon as the large cage occupancy has reached a threshold and starts involving double occupancy, the sII structure is energetically more favorable than the sI structure. Both nitrogen and carbon monoxide sI hydrate are significantly destabilized with increasing the double occupancy of the large cages. The larger size of the sII LCs[1] facilitates the encapsulation of two guest molecules per cage because of higher repulsive forces for two guest molecules in sI-LC when compared to sII-LC. Finally, the calculations have evidenced the need to consider the water-water interactions to describe the structural stability of the hydrate. Indeed, the aqueous network may undergo some deformations when hosting more than one guest molecule within the cages. The more deformed the water structure, the higher the host-host energy. Since water constitutes the major part of the hydrate structure, its contribution to the stabilization energy of the system is of prime importance.

The present study allowed to evidence the influence of the cage occupancy on the structural and energy properties of the nitrogen hydrate. The importance of considering both water-water and water-guest interactions to evaluate the structural stability of the hydrate has been highlighted.

ASSOCIATED CONTENT

Supporting Information.

The following files are available free of charge.

Additional DFT-derived data regarding the lattice parameters and the calculated energies. (PDF)

AUTHOR INFORMATION

The authors declare no competing financial interests.

FUNDING SOURCES

This paper falls in the frame of the MI2C project funded by the French ANR “Agence Nationale de la Recherche” (No. ANR-15CE29-0016)..

ACKNOWLEDGMENT

Calculations have been performed thanks to the computing center “Mésocentre de Calcul” at the “Université de Franche-Comté, France”.

REFERENCES

[1] Sloan, E. D.; Koh, C. A. *Clathrate Hydrates of Natural Gases. 3rd ed*; Taylor & Francis-CRC Press: Boca Raton, FL, 2008.

[2] *Gas Hydrates 1: Fundamentals, Characterization and Modeling;* Broseta, D., Ruffine, L., Desmedt, A., Eds.; Wiley-ISTE: London, UK, 2017.

[3] *Gas Hydrates 2: Geosciences and Applications;* Ruffine, L., Broseta, D., Desmedt, A., Eds.; Wiley-ISTE: London, UK, 2018.

[4] Qin, J.; Kuhs, W. F. Calibration of Raman Quantification Factors of Guest Molecules in Gas Hydrates and Their Application to Gas Exchange Processes Involving N_2. *J. Chem. Eng. Data* **2015,** *60*, 369-375.

[5] Pauer, F.; Kipfstuhl, J.; Kuhs, W. F. Raman Spectroscopic Study on the Nitrogen Ratio in Natural Ice Clathrates in the GRIP Ice Core. *Geophys. Res. Lett.* **1995,** *22*, 969-971.

[6] Pauer, F.; Kipfstuhl, J.; Kuhs, W. F. Raman Spectroscopic Study on the Spatial Distribution of Nitrogen and Oxygen in Natural Ice Clathrates and their Decomposition to Air Bubbles. *Geophys. Res. Lett*. **1996,** *23*, 177-180.

[7] Champagnon, B.; Panczer, G.; Chazallon, B.; Arnaud, L.; Duval, P.; Lipenkov, V. Nitrogen and Oxygen Guest Molecules in Clathrate Hydrates: Different Sites Revealed by Raman Spectroscopy. *J. Raman Spectrosc.* **1997,** *28*, 711-715.

[8] Kuhs, W. F.; Chazallon, B.; Radaelli, P. G.; Pauer, F. Cage Occupancy and Compressibility of Deuterated N_2-Clathrate Hydrate by Neutron Diffraction. *J. Incl. Phenom. Mol. Recognit. Chem.* **1997,** *29*, 65-77**.**

[9] Chazallon, B.; Champagnon, B.; Panczer, G.; Pauer, F.; Klapproth, A.; Kuhs, W. F. Micro-Raman Analysis of Synthetic Air Clathrates. *Eur. J. Mineral.* **1998,** *10*, 1125-1134.

[10] Chazallon, B.; Kuhs, W. F. In-Situ Structural Properties of N_2-, O_2- and Air-Clathrates by Neutron Diffraction. *J. Chem. Phys*. **2002,** *117*, 308-320.

[11] Lectez, S.; Simon, J.-M.; Mousis, O; Picaud, S.; Altwegg, K.; Rubin, M.; Salazar, J. M. A ∼32-70 K Formation Temperature Range for The Ice Grains Agglomerated by Comet 67P/Churyumov-Gerasimenko. *Astrophys. J., Lett.* **2015,** *805*: L1.

[12] Lundgaard, L.; Mollerup, J. Calculation of Phase Diagram of Gas Hydrates. *Fluid Phase Equilib*. **1992,** *76*, 141-149**.**

[13] Petuya, C.; Damay, F.; Chazallon, B.; Bruneel, J-L.; Desmedt, A. Guest Partitioning and Metastability of the Nitrogen Gas Hydrate. *J. Phys. Chem*. C **2018,** *122*, 566-573.

[14] Zhu, J.; Du, S.; Yu, X.; Zhang, J.; Xu, H.; Vogel, S. C.; Germann, T. C.; Francisco, J. S.; Izumi, F.; Momma, K, et al. Encapsulation Kinetics and Dynamics of Carbon Monoxide in Clathrate Hydrate. *Nat. commun.* **2014,** *5*, 4128.

[15] Petuya, C.; Damay, F.; Talaga, D.; Desmedt, A. Guest Partitioning in Carbon Monoxide by Raman Spectroscopy. *J. Phys. Chem. C* **2017,** *121*, 13798-13802.

[16] Sugahara, K.; Tanaka, Y.; Sugahara, T.; Ohgaki, K. Thermodynamic Stability and Structure of Nitrogen Hydrate Crystal. *J. Supramol. Chem.* **2002,** *2*, 365-368.

[17] Marshall, D.R., Saito, S.; Kobayashi, R. Hydrates at High Pressures: Part I. Methane-Water, Argon-Water, and Nitrogen-Water Systems. *AIChE J.* **1964,** *10*, 202-205.

[18] van Cleeff, A.; Diepen, G. A. M. Gas Hydrates of Nitrogen and Oxygen. Recl. Trav. Chim. Pays-Bas **1960,** *79*, 582-598.

[19] Hansen, T. C.; Falenty, A.; Kuhs, W. F. Lattice Constants and Expansivity of Gas Hydrates From 10 K up to the Stability Limit. *J. Chem. Phys*. **2016,** *144*, 054301.

[20] Petuya, C.; Damay, F.; Desplanche, S.; Aupetit, C.; Desmedt A. Ageing and Langmuir Behavior of the Cage Occupancy in the Nitrogen Gas Hydrate. Crystals **2018**, *8*, 145.

[21] Kuhs, W. F.; Chazallon, B.; Klapproth, A.; Pauer, F. Filling-Isotherms in Clathrate Hydrates. *Rev. High Pressure Sci. Technol.* **1998,** *7*, 1147-1149.

[22] Sasaki, S.; Hori, S.; Kume, T.; Shimizu, H. Microscopic Observation and In-Situ Raman Scattering Studies on High-Pressure Phase Transformations of a Synthetic Nitrogen Hydrate. *J. Chem. Phys*. **2003,** *118*, 7892-789.

[23] van Klaveren, E. P.; Michels, P. J.; Schouten, J. A.; Klug, D. D.; Tse, J. S. Stability of Doubly Occupied N_2 Clathrate Hydrates Investigated by Molecular Dynamics Simulations. *J. Chem. Phys.*, **2001,** *114*, 5745-5754.

[24] van Klaveren, E. P.; Michels, P. J.; Schouten, J. A.; Klug, D. D.; Tse, J. S. Molecular Dynamics Simulation Study of The Properties of Doubly Occupied N_2 Clathrate Hydrates. *J. Chem. Phys.*, **2001,** *115*, 10500-10508.

[25] Patt, A.; Simon, J.-M.; Picaud, S.; Salazar, J. M. A Grand Canonical Monte-Carlo Study of the N_2, CO and Mixed N_2-CO Clathrate Hydrates. *J. Phys. Chem. C*, **2018,** *122*, 18432-18444.

[26] Ballenegger, V. Cage Occupancies in Nitrogen Clathrate Hydrates from Monte Carlo Simulations. *J. Phys. Chem. C*, **2019**, *123*, 16757-16765.

[27] Desmedt, A.; Bedouret, L.; Pefoute, E.; Pouvreau, M.; Say-Liang-Fat, S.; Alvarez, M. Energy Landscape of Clathrate Hydrates. *Eur. Phys. J. Special Topics* **2012**, *213*, 103-127.

[28] Cox, S. J.; Towler, M. D.; Alfè, D.; Michaelides, A. Benchmarking the Performance of Density Functional Theory and Point Charge Force Fields in Their Description of SI Methane Hydrate Against Diffusion Monte Carlo. *J. Chem. Phys.* **2014,** *140*, 174703**.**

[29] Chakraborty, S. N.; English, N. J. Hydrogen-Bond Vibrational and Energetic Dynamical Properties in SI and SII Clathrate Hydrates and in Ice Ih: Molecular Dynamic Insights. *J. Chem. Phys.* **2015,** *143*, 154504.

[30] Desmedt, A.; Stallmach, F.; Lechner, R. E.; Cavagnat, D.; Lassègues, J. C.; Guillaume, F.; Grondin, J.; Gonzalez, M. A. Proton Dynamics in the Perchloric Acid Clathrate Hydrate $HClO_4$-5.5H_2O. *J. Chem. Phys.* **2004**, *121*, 11916-11926.

[31] Desmedt, A.; Lechner, R.E.; Lassègues, J.C.; Guillaume, F.; Cavagnat, D.; Grondin, J. Hydronium Dynamics in the Perchloric Acid Clathrate Hydrate. *Solid State Ionics* **2013**, *252*, 19-25.

[32] Bedouret, L.; Judeinstein, P.; Ollivier, J.; Combet, J.; Desmedt, A. Proton Diffusion in the Hexafluoro-phosphoric Acid Clathrate Hydrate. *J. Phys. Chem. B* **2014**, *118*, 13357-13364.

[33] Desmedt, A.; Martin-Gondre, L.; Nguyen, T. T.; Pétuya, C.; Barandiaran, L.; Babot, O.; Toupance, T.; Grim, R. G.; Sum, A. K. Modifying the Flexibility of Water Cages by Co-Including Acidic Species Within Clathrate Hydrates. *J. Phys. Chem. C* **2015**, *119*, 8904-8911.

[34] Nguyen, T. T.; Petuya, C.; Talaga, D.; Desmedt, A. Promoting the Insertion of Molecular Hydrogen in Tetrahydrofuran Hydrate with The Help of Acidic Additives, *Front. Chem.* **2020**, *8*, 550862.

[35] Burke, K. Perspective on Density Functional Theory. *J. Chem. Phys.* **2012,** *136*, 150901.

[36] Klimes, J.; Michaelides, A. Perspective: Advances and Challenges in Treating van Der Waals Dispersion Forces in Density Functional Theory. *J. Chem. Phys.* **2012,** *137*, 120901.

[37] Gillan, M. J.; Alfè, D.; Michaelides, A. Perspective: How Good is DFT for Water? *J. Chem. Phys.* **2016,** *144*, 130901.

[38] Vlasic, T. M.; Servio, P.; Rey, A. D. Atomistic Modeling of Structure II Gas Hydrate Mechanics: Compressibility and Equations of State. *AIP Adv.* **2016,** *6*, 085317**.**

[39] Petuya, C.; Martin-Gondre, L.; Aurel, P.; Damay, F.; Desmedt, A. Unraveling the Metastability Of the SI and SII Carbon Monoxide Hydrate with A Combined DFT-Neutron Diffraction Investigation. *J. Chem. Phys.* **2019,** *150*, 184705**.**

[40] Perdew, J. P.; Burke, K.; Ernzerhof, M. Generalized Gradient Approximation Made Simple. *Phys. Rev. Lett.* **1996,** *77*, 3865-3868.

[41] Dion, M.; Rydberg, H.; Schröder, E.; Langreth, D. C.; Lundqvist, B. I. Van der Waals Density Functional for General Geometries. *Phys. Rev. Lett.* **2004**, *92*, 246401.

[42] Kresse, G.; Hafner, J. Ab Initio Molecular Dynamics for Liquid Metal. *Phys. Rev. B* **1993**, *47*, 558-561.

[43] Kresse, G.; Hafner, J. Ab Initio Molecular Dynamics for Open-Shell Transition Metals. *Phys. Rev.* B **1993**, *48*, 13115-13118.

[44] Kresse, G.; Furthmüller, J. Efficiency of ab Initio Total Energy Calculations for Metals and Semi-Conductors Using Plane-Wave Basis Set. *Comput. Mater. Sci.* **1996**, *6*, 15-50.

[45] Kresse, G.; Furthmüller, J. Efficient Iterative Scheme for ab Initio Total-Energy Calculations Using Plane-Wave Basis Set. *Phys. Rev. B* **1996**, *54*, 11169-11186.

[46] Blöchl, P. E. Projector Augmented-Wave Method. *Phys. Rev. B* **1994,** *50*, 17953-17979.

[47] Kresse, G.; Joubert, J. From Ultrasoft Pseudopotentials to the Projector Augmented-Wave Method. *Phys. Rev. B*, **1999,** *59*, 1758-1775.

[48] Stackelberg, M. V.; Müller, H. R. Feste Gas Hydrate II: Struktur und Raumhemire", *Z. Elektrochem.* **1954,** *58*, 25-39.

[49] Udachin, K. A.; Ratcliffe, C. I.; Ripmeester, J. A. Structure, Composition and Thermal Expansion of CO_2 Hydrate from Single Crystal X-Ray Diffraction Measurements. *J. Phys. Chem. B* **2001,** *105*, 4200-4204.

[50] Takeuchi, F.; Hiratsuka, M.; Ohmura, R.; Alavi, S.; Sum, A. K.; Yasuoka, K. Water Proton Configurations in Structures I, II, and H Clathrate Hydrate Unit Cells. *J. Chem. Phys*. **2013,** *138*, 124504.

[51] Birch, F. Finite Elastic Strain of Cubic Crystals. *Phys. Rev.* **1947,** *71*, 809-824**.**

Table of Contents Graphics image